PROCEEDINGS OF SCIENCE

Exploring the phase space of jet splittings in pp and Pb–Pb collisions with ALICE

Nima Zardoshti* **for the ALICE Collaboration**
CERN and University of Birmingham
E-mail: nima.zardoshti@cern.ch

We report a series of recent jet substructure measurements made at ALICE, obtained using reclustering techniques. A variety of reclustering algorithms have been employed, with particular emphasis on the Soft Drop grooming procedure. The aim of these analyses are to experimentally access the splittings of the parton shower. Jet shapes are then constructed based on the splitting axes returned by the reclustering algorithms. In pp collisions, these are used to differentially probe fundamental QCD effects and validate PYTHIA at $\sqrt{s} = 7$ TeV. In central Pb–Pb collisions at $\sqrt{s_{\mathrm{NN}}} = 2.76$ TeV, these measurements are sensitive to quenching effects in the medium and probe the finer details of the energy loss mechanisms. The measurements presented include the following jet shapes: the ratio of 2-Subjettiness to 1-Subjettiness (τ_2/τ_1), the opening angle between the two axes of the 2-Subjettiness jet shape (ΔR), the momentum fraction carried by the subleading subjet in the first splitting satisfying Soft Drop (z_g) and the number of splittings in the jet tree which fulfil the Soft Drop criterium.

International Conference on Hard and Electromagnetic Probes of High-Energy Nuclear Collisions
30 September - 5 October 2018
Aix-Les-Bains, Savoie, France

*Speaker.

PoS(HardProbes2018)027

1. Introduction

Jets are collimated bunches of hadrons resulting from the fragmentation of partons scattered with high virtuality Q^2 in the initial stages of the collision. Reconstructed jets are the best experimental proxies for these initial scattered partons. In central heavy-ion collisions, where a dense medium of deconfined partons known as a Quark-Gluon Plasma (QGP) is expected to form, parton-medium interactions induce energy loss in the traversing partons. This results in a modification of the final state hadron distribution, compared to the vacuum. In particular, changes to the fragmentation pattern of the parton shower can provide detailed information on the mechanisms of this energy loss. To this end, a new class of jet shapes have been devised, which are sensitive to the medium-induced modifications of the splittings of the jet tree. The splittings are experimentally accessed by reclustering the jet with a given jet finding algorithm. The reclustering history can then be unwound to obtain the structures that were brought together in reverse order. The axes of these subjets are a proxy for the splittings of the parton shower.

2. Reclustering algorithms

Different choices of reclustering algorithm return axes that are proxies for splittings occurring at different scales. In this way, the multi-scale problem of jet showers can be systematically addressed. The reclustering algorithms used here are as follow:

2.1 Exclusive k_{T}

The exclusive k_{T} algorithm [1] takes into account the p_{T} and angular separation of constituent pairs and begins by clustering soft particles that are separated by small angles. In the final step of this procedure, two hard substructures are brought together. In this way, unwinding the k_{T} algorithm one step returns a hard splitting.

2.2 Cambridge/Aachen

The C/A algorithm [2] clusters particles based solely on their angular separation. Particles closest to each other are combined first, with the final step of the algorithm bringing together the furthest separated structure in the jet. Unwinding this procedure results in the widest splitting being returned. The lack of p_{T} weighting in the reclustering procedure results in a sensitivity to large angle radiation, which is predominantly soft. This type of radiation can originate from the underlying event, particularly in central heavy-ion collisions. Therefore, two modifications to the default C/A reclustering are also considered.

2.3 Cambridge/Aachen with a one-pass minimisation

The first modification involves a one-pass minimisation procedure [3], starting from the axes returned by the C/A reclustering. The minimisation is performed by geometrically varying these axes to find a local minimum of N-subjettiness. Such a procedure is expected to reduce the sensitivity of the reclustering to large angle soft radiation. The extent of this will be determined experimentally.

2.4 Soft Drop grooming

The second modification is the application of the Soft Drop groomer [4] on the C/A reclustered tree. Instead of accepting the axes returned by unwinding the reclustering procedure one step, they are first tested against the Soft Drop condition. This is given by

$$\frac{min(p_{\mathrm{T}}^{a}, p_{\mathrm{T}}^{b})}{p_{\mathrm{T}}^{a} + p_{\mathrm{T}}^{b}} > z_{\mathrm{cut}}(\frac{\Delta R_{ab}}{R_0})^{\beta}, \tag{2.1}$$

where the labels a and b refer to the subjets returned by the reclustering algorithm. ΔR_{ab} is the angular distance between the subjet axes in the $\eta - \varphi$ (pseudorapidity-azimuth) plane. The z_{cut} and β parameters control the grooming procedure and are the minimum momentum fraction carried by the subleading subjet and the degree of interplay between the angular and momentum components of the splitting respectively. If a splitting satisfies the Soft Drop criterium, it is returned. However, if the splitting does not meet the requirements, the subleading subjet is groomed away and the reclustering history of the remaining subjet is unwound. The resultant splitting is again tested against the Soft Drop condition. This process is repeated until either a suitable splitting is found or until all structures have been groomed away and only a single track remains. In this case the jet is discarded.

3. Jet shapes

The N-subjettiness jet shape [5], τ_N, where N can be any positive integer, is a measure of how strongly N-prong a jet's substructure is. It is defined by

$$\tau_N = \frac{1}{R p_{\mathrm{T}}^{\mathrm{jet}}} \sum_i p_{\mathrm{T}}^{i} min(\Delta R_{1,i}, \Delta R_{2,i}, ..., \Delta R_{N,i}), \tag{3.1}$$

where the subscript i denotes each track in the jet and N is the number of axes found by declustering the jet $N-1$ steps. Jets with N or fewer well defined cores have τ_N values approaching 0, whereas jets which are comprised of at least $N+1$ substructures have τ_N values approaching unity. The discrimination for exactly N cores in the jet is obtained via the ratio τ_N/τ_{N-1}. In this way, τ_2/τ_1 is a jet shape sensitive to two-prong jets. Therefore, this variable can provide information on quenching mechanisms that alter the two-prong probability of jets traversing the QGP medium, relative to vacuum. These can include colour coherence effects [6] (suppression of two-prong jets) or semi-hard medium-induced radiation (enhancement of two-prong jets [7]).

The opening angle between the two axes in the calculation of τ_2 is also a jet shape, which can exhibit sensitivity to coherence effects. It is denoted by ΔR, which is given by

$$\Delta R_{1,2} = \sqrt{(\eta_1 - \eta_2)^2 + (\varphi_1 - \varphi_2)^2}. \tag{3.2}$$

The Soft Drop groomer also yields a series of measurable jets shapes. The first of these is defined relative to the first splitting that passes the Soft Drop condition. This is the momentum fraction carried by the subleading subjet, z_g. The next shape, n_{SD}, is obtained by iteratively following the reclustering history through the hardest subjet at each branch and counting the total number

of splittings that pass the Soft Drop condition. Medium modifications to these variables can indicate changes to the QCD splitting functions in the QGP. The Soft Drop procedure employed in these analyses, was implemented with $z_{cut} = 0.1$ and $\beta = 0$. This removes the angular dependence of the grooming and is sensitive to hard and semi-hard splittings.

4. Analysis procedure

In both the pp ($\sqrt{s} = 7$ TeV) and Pb–Pb ($\sqrt{s_{NN}} = 2.76$ TeV) collision systems the datasets were acquired using a minimum bias trigger, with an online centrality selection used in Pb–Pb collisions to pick the 0–10% most central events. Jet finding was performed on charged tracks, using the anti-k_{T} algorithm with a jet resolution of $R = 0.4$ using the FastJet package [8]. Minimum and maximum constituent $p_{\mathrm{T}}^{\mathrm{ch}}$ limits of 0.15 and 100 GeV/c, respectively, were also imposed. The jet cone was required to be fully within the confines of the ALICE central barrel [9] ($|\eta| \leq 0.9$), meaning that $|\eta_{\mathrm{jet}}| \leq 0.5$.

The large background, due to the underlying event in central Pb–Pb collisions, necessitates additional measures to increase the signal to background ratio. Jets with an area less than 60% of a cone with radius of 0.4 were discarded. This suppressed background jets whilst keeping true jets with a high efficiency. Background subtraction techniques were also applied to remove the average event-wise background from the p_{T} and jet shapes. The main method used was the constituents subtraction method [10] with the derivatives method [11] employed as a systematic cross check.

The performances of the background subtraction techniques were evaluated using an embedding procedure. Particle level PYTHIA [12] jets were generated and propagated to detector level using GEANT3. These detector level jets were subsequently embedded into real 0–10% most central Pb–Pb events and jet finding was performed in the presence of the heavy-ion background. Background subtraction techniques were then applied to the embedded level jets. The subtracted embedded level jets were matched to the particle level PYTHIA jets. It was found that the subtraction procedures worked well for the τ_2/τ_1 jet shape. However, the ΔR and z_g distributions showed a high level of sensitivity to local fluctuations in the background which remained even after subtraction. This inhibited successful unfolding of these shapes.

In order to simultaneously correct the $p_{\mathrm{T}}^{\mathrm{jet,ch}}$ and jet shapes for detector effects (pp and Pb–Pb) and background fluctuations (Pb–Pb), a two-dimensional Bayesian unfolding procedure [13] was employed. This procedure required a pure sample of true jets as an input, since the constructed response matrices did not account for combinatorial (background originating) jets. In pp collisions this sample of jets was obtained by imposing a $p_{\mathrm{T}}^{\mathrm{jet,ch}} \geq 10$ GeV/c cut. However in Pb–Pb collisions, large local fluctuations in the background meant that combinatorial jets were still significantly present at higher $p_{\mathrm{T}}^{\mathrm{jet,ch}}$ values. To this end, the semi-inclusive hadron-jet coincidence (recoil) method [14] was applied to obtain a combinatorial free distribution of jets. Two high $p_{\mathrm{T}}^{\mathrm{ch}}$ trigger hadron classes of 15–45 GeV/c (signal) and 8–9 GeV/c (reference) were defined and jet finding was performed in an azimuthally back to back window to the trigger hadrons. The contribution of combinatorial jets is expected to be uncorrelated to the trigger hadrons and hence equal between both classes. Subtracting the signal and reference distributions removed the contribution of combinatorial jets and resulted in a combinatorial free distribution which formed the input to the unfolding procedure. This method allowed the obtention of a distribution of true jets, without

imposing any fragmentation bias on the recorded jet population. Other trigger hadron induced biases have been shown to saturate at the p_{T} classes considered here and were therefore eliminated through the subtraction procedure. This method was extended to two dimensions for the simultaneous unfolding of the $p_{\mathrm{T}}^{\mathrm{jet,ch}}$ and jet shapes.

5. Results

The final results pertaining to the measured jet shapes are presented for each collision system. In pp collisions, all shapes were fully corrected down to particle level, through Bayesian unfolding. In Pb–Pb collisions, only the (recoil) τ_2/τ_1 shape was unfolded. The remainder of the shapes are presented at the (inclusive) background subtracted uncorrected level. Where unfolding was possible, the fully corrected results are presented in the $40 \leq p_{\mathrm{T}}^{\mathrm{jet,ch}} < 60$ GeV/c bin and compared with particle level PYTHIA. Where unfolding was not possible, the measured distributions are presented at $80 \leq p_{\mathrm{T}}^{\mathrm{jet,ch}} < 120$ GeV/c, to mitigate against combinatorial jets. These uncorrected results are compared to subtracted embedded distributions, which faithfully reproduce all background and detector effects. In Pb–Pb collisions, any potential differences between the compared distributions can be attributed to quenching effects.

5.1 pp

The fully corrected τ_2/τ_1 and ΔR jet shapes in pp collisions at $\sqrt{s} = 7$ TeV, obtained for each reclustering algorithm, are shown in Fig. 1 and 2 respectively. The τ_2/τ_1 distributions obtained with the k_{T} and Soft Drop reclustering procedures peak at intermediate values, indicating that these algorithms are sensitive to hard substructures within the jet. The ΔR distributions for these algorithms peak at small values, indicating that the majority of hard substructures exist within the core of the jet. This is in agreement with the primarily single-cored nature of QCD jets. In contrast, the τ_2/τ_1 distributions obtained with the C/A algorithm, with and without minimisation, tend towards unity. This indicates that the second axis in the τ_2 case is not aligned with any significant fraction of $p_{\mathrm{T}}^{\mathrm{ch}}$ in the jet. The corresponding ΔR distributions tend towards the jet radius, indicating that soft scale splittings occur at large angles in the jet. All shapes are well described by PYTHIA with the Perugia 11 tune [15], with the axes themselves (ΔR) described better than the fragmentation of constituents around the axes (τ_2/τ_1).

The fully corrected Soft Drop variables, z_g and n_{SD}, are shown in Fig. 3. These shapes are well described by PYTHIA Perugia 11. Instead of normalising the distributions to the total number of entires (jets) in each plot, as in the case for τ_2/τ_1 and ΔR, these distributions are normalised to the total number of jets in the reconstructed $p_{\mathrm{T}}^{\mathrm{ch}}$ bin. This has a significant effect on the corresponding z_g shapes measured in Pb–Pb, as they render the distributions sensitive to a change in rate rather than a change in shape.

5.2 Pb–Pb

The fully corrected recoil τ_2/τ_1 distributions in Pb–Pb collisions at $\sqrt{s_{\mathrm{NN}}} = 2.76$ TeV, obtained for each reclustering algorithm, are shown in Fig. 4. For all algorithms a good agreement is seen between PYTHIA Perugia 11 and the unfolded results, indicating that no quenching effects are discernible. The same physics arguments made for the pp case apply.

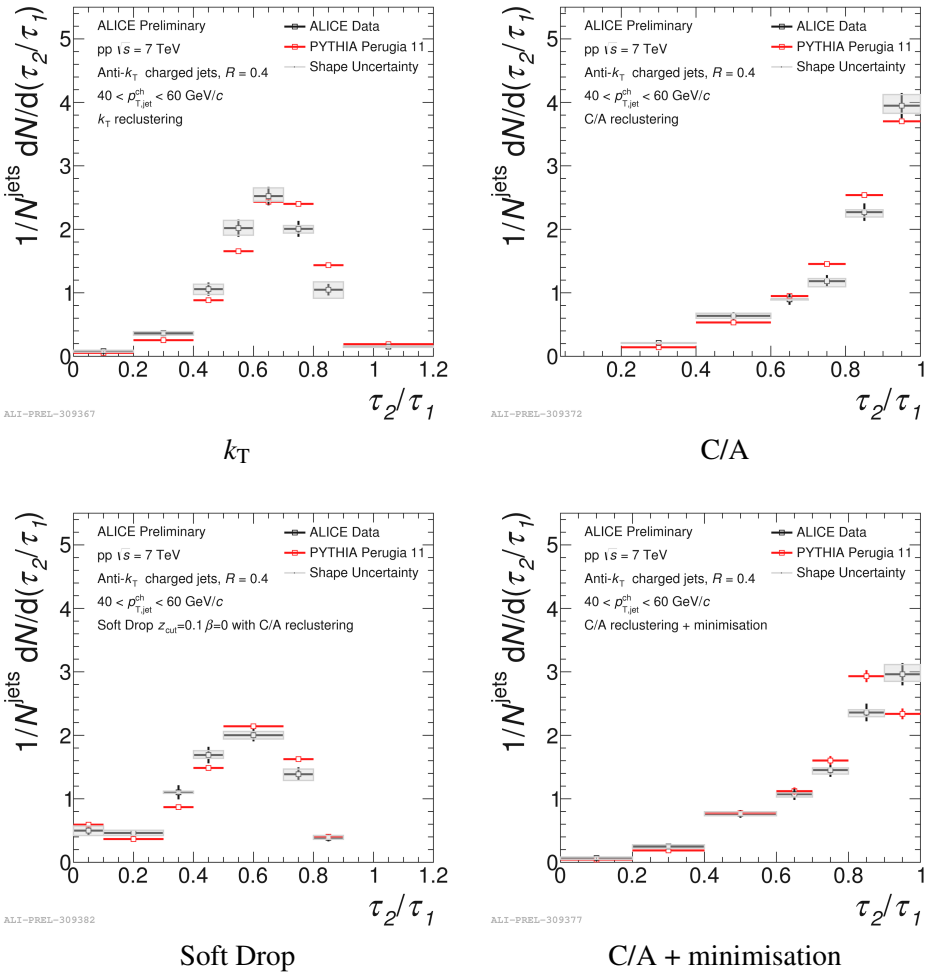

Figure 1: The fully corrected τ_2/τ_1 distributions for different reclustering algorithms, measured in pp collisions at $\sqrt{s} = 7$ TeV, are shown. The jets have a resolution of $R = 0.4$ at $40 \leq p_{\mathrm{T}}^{\mathrm{jet,ch}} < 60$ GeV/c. Comparisons to PYTHIA Perugia 11, at the corresponding centre-of-mass energy, have also been provided.

The (uncorrected) background subtracted inclusive z_g results are shown in Fig. 5, for different cuts on the opening angle (ΔR) of the splitting. Collimated splittings show an enhancement at low z_g relative to the embedded distributions, whilst large angle splittings are suppressed at high z_g. For splittings with $\Delta R > 0.1$, no net enhancement is observed, relative to the embedded sample. The n_{SD} jet shape, shown in Fig. 6, also shows no net enhancement in the number of splittings passing Soft Drop.

6. Conclusion

The τ_2/τ_1 and ΔR shapes have been presented for a series of different reclustering algorithms, probing different scales of the jet shower. The results across all algorithms exhibit no medium-induced modifications. These shapes, particularly the ones obtained using the k_{T} and Soft Drop procedures, would be susceptible to the addition or suppression of a hard or semi-hard prong in

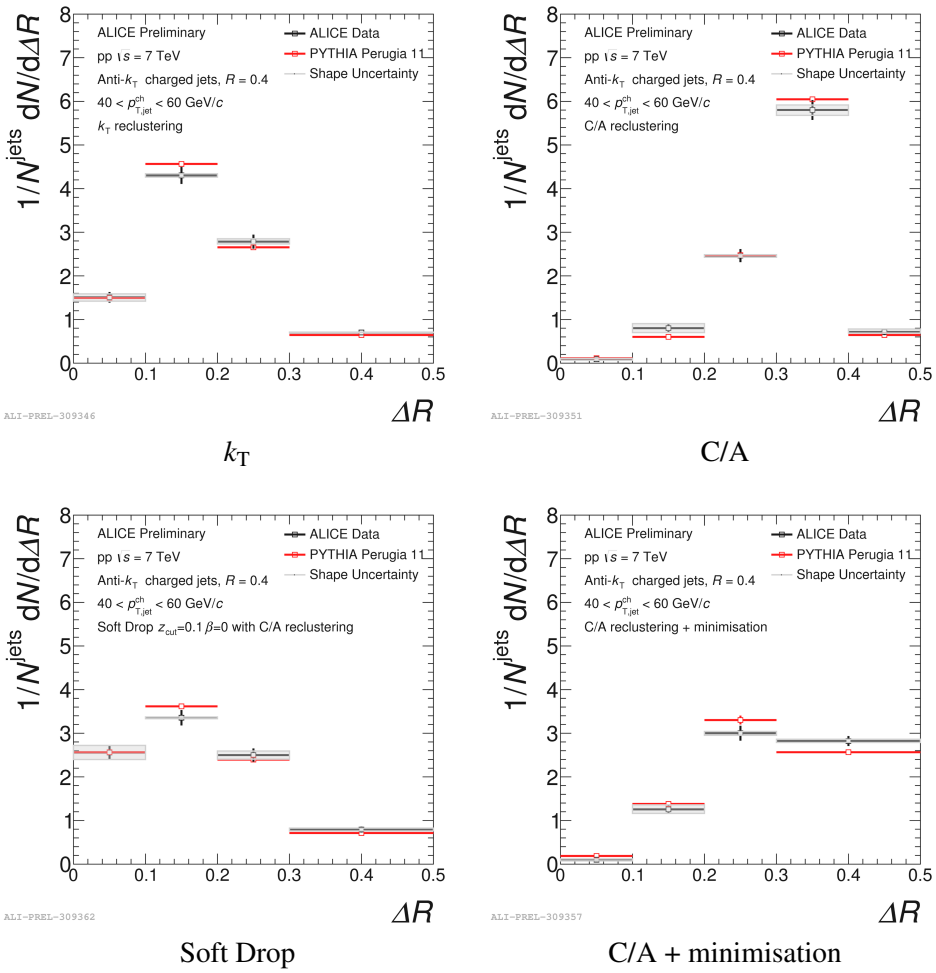

Figure 2: The fully corrected ΔR distributions for different reclustering algorithms, measured in pp collisions at $\sqrt{s} = 7$ TeV, are shown. The jets have a resolution of $R = 0.4$ at $40 \leq p_{\mathrm{T}}^{\mathrm{jet,ch}} < 60$ GeV/c. Comparisons to PYTHIA Perugia 11, at the corresponding centre-of-mass energy, have also been provided.

the jet, due to medium-induced radiation and coherence effects respectively. The z_g distributions show a significant modification in the medium, with large angle splittings suppressed. However, the number of hard splittings, n_{SD}, shows no net enhancement in medium compared to vacuum.

Full interpretation of these results, alongside other measured jet shapes sensitive to quenching, requires further work in the community. The differential nature of the jet substructure program at ALICE aims to provide a series of complementary measurements which can be used to probe the finer details of the medium-induced energy loss.

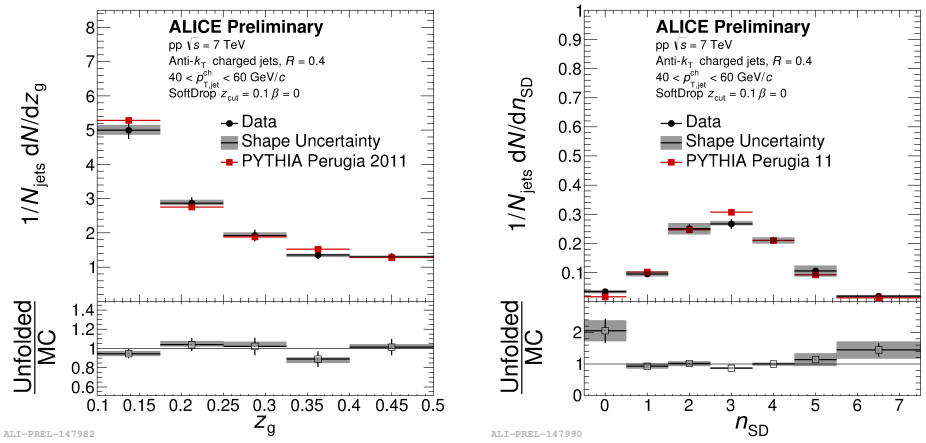

Figure 3: The fully corrected z_g and n_{SD} distributions, measured in pp collisions at $\sqrt{s} = 7$ TeV, are shown. The jets have a resolution of $R = 0.4$ at $40 \leq p_{\mathrm{T}}^{\mathrm{jet,ch}} < 60$ GeV/c. Comparisons to PYTHIA Perugia 11, at the corresponding centre-of-mass energy, have also been provided.

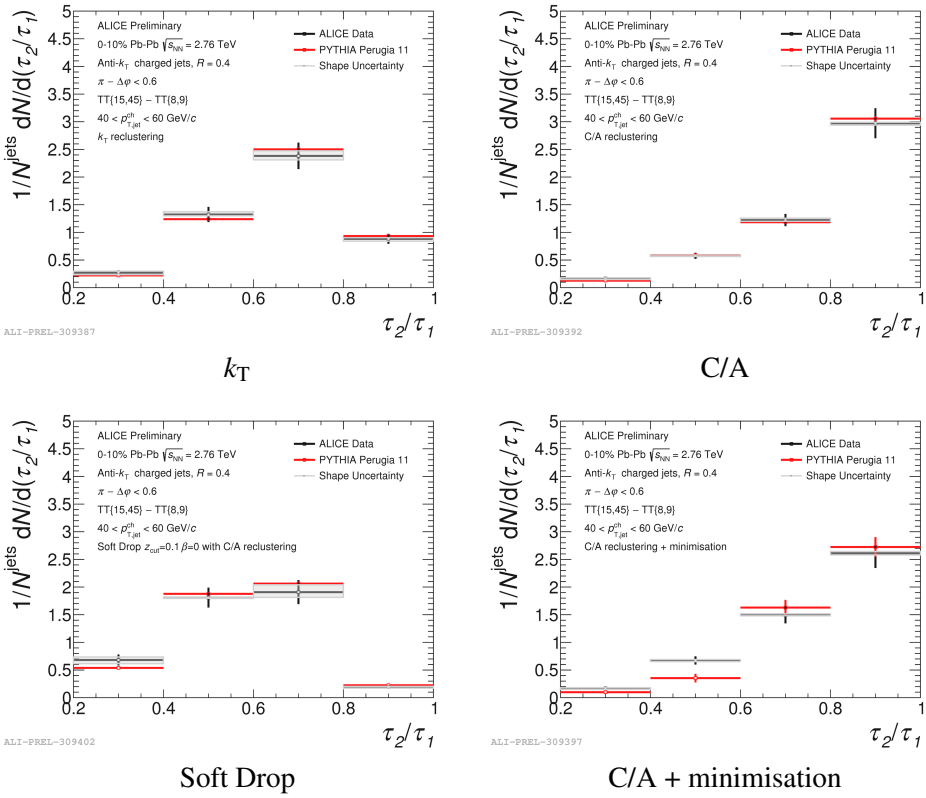

Figure 4: The fully corrected recoil τ_2/τ_1 distributions for different reclustering algorithms, measured in the 0–10% most central Pb–Pb collisions at $\sqrt{s_{\mathrm{NN}}} = 2.76$ TeV, are shown. The jets have a resolution of $R = 0.4$ at $40 \leq p_{\mathrm{T}}^{\mathrm{jet,ch}} < 60$ GeV/c. Comparisons to (recoil) PYTHIA Perugia 11, at the corresponding centre-of-mass energy, have also been provided.

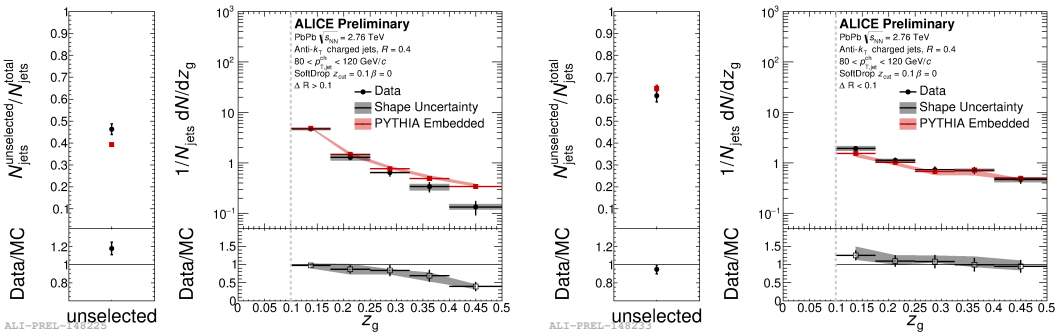

$\Delta R > 0.1$ $\Delta R < 0.1$

Figure 5: Constituent subtracted inclusive distributions of z_g, measured in the 0–10% most central Pb–Pb collisions at $\sqrt{s_{\mathrm{NN}}} = 2.76$ TeV, are shown for different cuts on the opening angle of the splitting. The jets have a resolution of $R = 0.4$ at $80 \leq p_{\mathrm{T}}^{\mathrm{jet,ch}} < 120$ GeV/c. Comparisons to embedded PYTHIA, at the corresponding centre-of-mass energy, have also been provided.

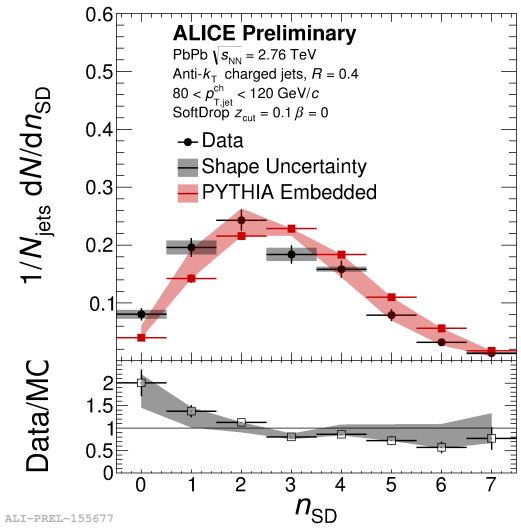

Figure 6: The constituent subtracted inclusive distribution of n_{SD}, measured in the 0–10% most central Pb–Pb collisions at $\sqrt{s_{\mathrm{NN}}} = 2.76$ TeV, is shown. The jets have a resolution of $R = 0.4$ at $80 \leq p_{\mathrm{T}}^{\mathrm{jet,ch}} < 120$ GeV/c. A comparison to embedded PYTHIA, at the corresponding centre-of-mass energy, has also been provided.

References

[1] S.D. Ellis and D.E. Soper, Phys.Rev. D48 (1993) 3160

[2] Yu.L. Dokshitzer, G.D. Leder,S. Moretti and B.R. Webber, JHEP 9708 (1997) 001

[3] J. Thaler and K.V. Tilburg, JHEP 1202 (2012) 093

[4] A.J. Larkoski, S. Marzani, G. Soyez and J. Thaler, JHEP 1405 (2014) 146

[5] J. Thaler and K.V. Tilburg, JHEP 1103 (2011) 015

[6] Y. Mehtar-Tani, C.A. Salgado and K. Tywoniuk, Phys.Rev.Lett. 106 (2011) 122002

[7] Y. Mehtar-Tani and K. Tywoniuk, JHEP 1704 (2017) 125

[8] M. Cacciari, G.P. Salam and G. Soyez, Eur.Phys.J. C72 (2012) 1896

[9] ALICE Collaboration, K. Aamodt et al., JINST 3 (2008) S08002

[10] P. Berta, M. Spousta and D.W. Miller, JHEP 1406 (2014) 092

[11] G. Soyez, G.P. Salam, J. Kim, S. Dutta and M. Cacciari, Phys.Rev.Lett. 110 (2013) no.16, 162001

[12] T. Sjostrand, S. Mrenna and P.Z. Skands, JHEP 0605 (2006) 026

[13] G. D'Agostini, Nucl.Instrum.Meth. A362 (1995) 487

[14] ALICE Collaboration, J. Adam et al., JHEP 1509 (2015) 170

[15] P.Z. Skands, Phys.Rev. D82 (2010) 074018